UNIVERSITETET I OSLO
UNIVERSITY OF OSLO

Absolute In Situ Energy Calibration of Luminosity Calorimeters in the DELPHI experiment at LEP

Lars Bugge Mogens Dam* A.L. Read*
Fysisk Institutt, Boks 1048,
Universitetet i Oslo, N-0316 Oslo, Norway

Jan Myrheim*
Institutt for fysikk,
NTH, N-7034 Trondheim, Norway

Geir Skjevling
Oslo Ingeniørhøgskole, N-0254 Oslo, Norway
July 22, 1992

UiO PHYS 92-20
ISSN-0332-5571

Received: 1992-07-27
OUP--92-20

FYSISK INSTITUTT
DEPARTMENT OF PHYSICS

Absolute In Situ Energy Calibration of Luminosity Calorimeters in the DELPHI experiment at LEP

Lars Bugge Mogens Dam* A.L. Read*
Fysisk Institutt, Boks 1048,
Universitetet i Oslo, N-0316 Oslo, Norway

Jan Myrheim*
Institutt for fysikk,
NTH, N-7034 Trondheim, Norway

Geir Skjevling
Oslo Ingeniørhøgskole, N-0254 Oslo, Norway
July 22, 1992

UiO PHYS 92-20
ISSN-0332-5571

Received: 1992-07-27

* Supported by the Norwegian Natural Science Research Council

Absolute *In Situ* Energy Calibration of Luminosity Calorimeters in the DELPHI experiment at LEP

Lars Bugge Mogens Dam*
A.L.Read*
Fysisk Institutt, Boks 1048,
Universitetet i Oslo, N–0316 Oslo, Norway

Jan Myrheim*
Institutt for fysikk,
NTH, N–7034 Trondheim, Norway

Geir Skjevling
Oslo Ingeniørhøgskole, N–0254 Oslo, Norway

July 22, 1992

Methods to perform the absolute energy calibration of DELPHI's Small Angle Tagger luminosity calorimeters at LEP are presented and compared. The input was small angle Bhabha scattering events. A significant non-linearity in the response of the calorimeters was observed. The conjugate gradient method was applied to solve the least squares problem. This method is particularly useful for least squares problems which are large, ill-behaved or even singular, and for cases with a sparse coefficient matrix.

*Supported by the Norwegian Natural Science Research Council

1 Introduction

The problem of energy calibration is common to all experiments where precise energy measurements are imperative. An outstanding example is the luminosity determination at e^+e^- colliders based on the counting of Bhabha events. In this article the case of the Small Angle Tagger calorimeters (SAT) of the DELPHI experiment at LEP is addressed. The luminosity analysis is described in [1] and, in more detail, in [2]. The importance of the energy calibration is illustrated by the fact that the bias in the luminosity measurement introduced by a 1% shift in the absolute energy scale around the energy cut is ~0.2%, to be compared to the quoted total systematic uncertainty on the luminosity of ~0.7% [2]. The luminosity is less sensitive to the energy *resolution* as it enters as a second order effect.

The SAT consists of two identical calorimeters, placed symmetrically around the nominal e^+e^- interaction point, with the entrance at $|z| = 232$ cm, where the z coordinate measures the distance along the beam. They consist of concentric cylindrical layers of lead sheets (thickness 0.9 mm) interleaved with 1mm diameter scintillating fibres. The cylinder axis coincides with the nominal beam line, thus the fibres are parallell to the beam. Inner and outer radii are 10 and 34.5 cm, respectively. The angular range covered is 43 to 135 mrad. The calorimeters are 28 X_0 (radiation lengths) long. Behind each calorimeter the fibres are gathered into 288 bundles. Each bundle is read out by a circular photodiode with 1 cm^2 active area via a conical light guide. One of the calorimeters (denoted calorimeter 2 in what follows) is equipped with lead masks in front of the inner ring of readout elements, and covering $\pm 15°$ from the vertical. The read-out element geometry is displayed in figure 1. The regions covered by the masks in calorimeter 2 are shaded. Further details can be found in references [3] and [4].

2 The data and the methods

The methods described in this section each uses one out of the four models given below for the energy E_j of cluster j.

$$E_j = \sum_{i=1}^{N_{clus}} c_i Q_{ij} \tag{1}$$

$$E_j = \sum_{i=1}^{N_{clus}} (c'_i \chi_{ij} + c_i Q_{ij}) \tag{2}$$

$$E_j = \sum_{i=1}^{N_{clus}} (c_i Q_{ij} + \zeta_i Q^2_{ij}) \tag{3}$$

$$E_j = \sum_{i=1}^{N_{clus}} (c'_i \chi_{ij} + c_i Q_{ij} + \zeta_i Q^2_{ij}) \tag{4}$$

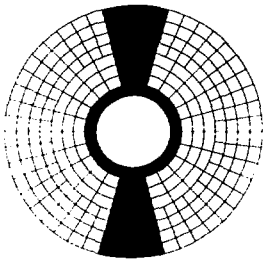

Figure 1: The geometrical arrangement of the read-out elements. The area covered by lead masks in calorimeter 2 is shaded.

The index i runs over the number $N_{elem} = 288$ of elements in the calorimeter. Q_{ij} denotes the pedestal corrected ADC signal of read-out element i in energy cluster j if element i is part of the cluster, $Q_{ij} = 0$ otherwise. χ_{ij} is defined by

$$\chi_{ij} \quad \begin{cases} 1 & \text{if element } i \text{ is in cluster } j, \\ 0 & \text{otherwise.} \end{cases} \tag{5}$$

Typical clusters contain 5 12 elements. The aim of the calibration procedures is to determine the best set of parameters constraining the average value $< E_j / E_j^{beam} >$ to equal 1.0 where E_j^{beam} denotes the value of the beam energy valid for energy cluster j. The data used in this paper cover a spectrum of beam energies in the range 44.3 46.9 GeV.

The parameters are the N_{elem} 288 calibration constants $(c_i)_1^{288}$ in case of the simple model 1. For model 2, which contains a possible offset for each element, the parameters are the $2N_{elem}$ constants $(c_i^0)_1^{288}$ and $(c_i)_1^{288}$. Model 3 includes a term quadratic in the ADC signal for each element and the parameters are the $2N_{elem}$ constants $(c_i)_1^{288}$ and $(\zeta_i)_1^{288}$. Model 4 includes both an offset term and a term quadratic in the ADC signal for each element, thus the parameters are the $3N_{elem}$ constants $(c_i^0)_1^{288}$, $(c_i)_1^{288}$, and $(\zeta_i)_1^{288}$. All four models are linear in the parameters.

The model of eq. 2 is justified by observations in SAT prototype tests that whereas the calorimeter module showed an excellent linearity, linear extrapola-

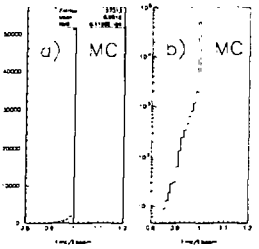

Figure 2: The spectrum of true energies in Monte Carlo for well contained events passing the cuts of the calibration algorithms. a): Linear scale, b): Logarithmic scale.

tions of ADC signals to zero energy showed significant non-zero results [4]. Models 3 and 4 are interesting in their own right, and in particular since detailed, high statistics comparisons of data to Monte Carlo indicate a slight non-linearity in the SAT energy response. It should be noted that the SAT detectors installed at LEP differ slightly from the prototype setup both concerning calorimeters and readout. Despite the fact that all the data are taken at very close beam energies the study of the quadratic model is *a priori* interesting since the individual element energies building up the clusters have a large spread all the way from close to the beam energy down to the minimim element energy cut of a few hundred MeV [2].

The input common to all the methods consisted of M 50000 Bhabha event energy clusters for each calorimeter. The clusters consisted of neighbouring readout elements' ADC' signals, corrected for the pedestals and provided the signals were above 3 sigma of the noise. Only energy clusters which, when combining the two calorimeters, passed the cuts of the Bhabha analysis were used. In addition, clusters with significant energy lost due to initial or final state radiation were rejected by applying a tight acolinearity cut of $|R_1 - R_2| < 1.5$ cm, and the energy cut was strengthened to $0.85E^{beam} < E < 1.15E^{beam}$. Here R_k denotes the cluster radial centre of gravity in calorimeter k, and E the cluster energy. Both R_k and E were calculated with calibration constants from a previous calibration. Figure 2 shows the true energy distribution for Monte Carlo [5] events passing these selection criteria. It is seen that the input events constitute a close to monoenergetic spectrum, ideal for the purpose of calibration.

In the following subsections the calibration algorithms are presented, and in

section 3 their performances are described and compared. The methods are two variants of a robust iterative method, referred to as methods IA and IB, and four variants of a least squares fit method, referred to as methods IIA, IIB, IIC, and IID. All the methods take calibration constants obtained by method IB in a previous calibration as a first estimate.

2.1 Method IA

This method was designed to be simple and robust. It uses the simple linear model of eq.1. The method is an iterative one which for each cluster in each iteration calculates the energy of the cluster including all elements except the one with maximum ADC signal, $\widetilde{E}_j = \sum_{i \neq i_{max}} c_i Q_{ij}$ using the calibration constants from the previous iteration. The maximum signal element is then assigned a new calibration constant $c_{i_{max}j} = (E_j^{beam} - \widetilde{E}_j)/Q_{i_{max}j}$ with weight $w_{i_{max}j} = E_{i_{max}}/E_j$, i.e. the fraction of the total cluster energy assigned to the maximum signal element. Both $E_{i_{max}}$ and E_j are calculated with the calibration constants from the previous iteration.

After the completion of one iteration, all elements which have at least once contained the maximum ADC signal of a cluster have got a new calibration constant. In general an element has been the one with maximum signal n times, and the new calibration constants after the completion of an iteration is the weighted mean $c_i = \sum_{l=1}^{n} w_{il} c_{il} / \sum_{l=1}^{n} w_{il}$. A new constant is considered significant and used as input to the next iteration only if its total weight $W_i = \sum_{l=1}^{n} w_{il}$ is greater than a predefined limit W_{min}. Furthermore, effects from non-Gaussian tails are minimized by only accepting new calibration constants in an iteration if they differ by less than twice the expected standard deviation from the previous iteration. This cut is not applied in the first iteration to allow for wrong starting point values.

Due to lead masking [1, 2] and leakage, elements in the inner- and outermost rings (see fig. 1) are not likely to become maximum signal elements. To assure recalibration of these elements the method was expanded to also treat the maximum signal element in the inner and outermost rings, when such elements were part of a cluster.

The procedure was stopped when convergence was reached or a predefined maximum number of iterations was passed. Convergence was defined as $\Delta s^2 < 10$ five times contiguously where Δs^2 is defined as the change in

$$s^2 = \sum_{j=1}^{M} (E_j^{beam} - E_j)^2 \qquad (6)$$

from the previous iteration

2.2 Method IB

This method is a modified version of Method IA. Instead of assigning only the maximum signal element in a cluster a new calibration constant, all elements in a cluster are assigned a new constant keeping the relative sizes of the element energies as given by the previous iteration. With the element weights defined as $w_{ij} = E_{ij}/E_j$ where E_{ij} is the element energy of element i in cluster j and E_j the cluster energy, both calculated with calibration constants from the previous iteration, the calibration constants assigned are $c_{ij} = w_{ij}E_j^{beam}/Q_{ij}$ and after completion of one iteration the resulting calibration constants are taken as the weighted means of the c_{ij}'s as for method IA. As in method IA the total weight was required to be above a limit, and non-Gaussian tail effects were avoided in the same way. Also convergence was defined the same way as in method IA.

2.3 Least Squares Methods

Motivated by the increased flexibility in the choice of model, the calibration task is formulated as a linear least squares problem. This easily allows the use of models like 2 4, or others, in the calibration.

The sum of squares to be minimized reads

$$F = \sum_{j=1}^{M} (E_j^{beam} - E_j)^2/\sigma^2 \tag{7}$$

with E_j expressed as a function of the readout elements' ADC signals according to the chosen model. A common measurement error σ on the energy measurement is assumed. In matrix notation the sum of squares can be written quite generally

$$F = \frac{1}{\sigma^2} e^t e \tag{8}$$

where ^{t} denotes transposed and e is the M-dimensional vector of residuals: $e = d - Hp$ where $d_j = E_j^{beam}, j = 1, \ldots, M$, p is the N dimensional vector of parameters to be fitted, and the $M \times N$ dimensional matrix H contains the model.

The standard way of solving the least squares problem for the case of a model linear in the parameters, is solving the equations

$$\frac{\partial F}{\partial p_k} = 0, \; k = 1, \ldots, N \tag{9}$$

or, in matrix notation,

$$H^t H p = H^t d \tag{10}$$

by inverting the $N \times N$ matrix $H^t H$. This matrix is, however, in many applications ill behaved and not invertible. An alternative approach to solving the least

squares problem is therefore applied. This approach is a simple adaptation of the conjugate gradient ...ethod for solving linear equations [6, 7, 8]. The method is described in sufficient detail for potential users in ref. [8]. It is robust with respect to the properties of H (or $H^T H$), and is little dependent on the values of N and M or the magnitude of the matrix elements. Thus the method is a better alternative than the traditional approach in many applications of least squares fitting in experimental physics. The calibration problem presented here is also characterized by a sparse coefficient matrix: out of the $N \times M$ matrix elements in H only a few are non-zero. Therefore multiplications with H or H^T are fast, and only a fraction of the elements of H needs to be stored. This is all taken advantage of in the conjugate gradient method.

The method is iterative and converges exactly in N iterations, although this property is usually only of theoretical interest, because of rounding errors. It may give sufficient convergence earlier, however, so after each iteration there should be a test for convergence. In the applications described in this article the iterations were stopped when the relative change in the sum of squares F (see eq. 7 and ref. 8.) from the previous iteration had been smaller than 10^{-5} five times contiguously. The maximum number of iterations was set to N. To avoid numerical overflow problems, the element signals $Q_{i,j}$ were multiplied by a factor 0.01.

Method IIA uses model 1, H_{ji} $Q_{i,j}$, i = 1,...288, N = 288, and the parameters are p_i c_i, i 1,...,288.

Method IIB uses model 2,

$$H_{ji} \quad \begin{cases} Q_{i,j} & \text{i } 1,\ldots,288 \\ \chi_{i\ 288,j} & \text{i } 289,\ldots,576 \end{cases}$$

N 576, and the parameters are

$$p_i \quad \begin{cases} c_i & \text{i } 1,\ldots,288 \\ c_{i\ 288} & \text{i } 289,\ldots,576 \end{cases}$$

Method IIC uses model 3,

$$H_{ji} \quad \begin{cases} Q_{i,j} & \text{i } 1,\ldots,288 \\ Q_{i\ 288,j}^2 & \text{i } 289,\ldots,576 \end{cases}$$

N 576, and the parameters are

$$p_i \quad \begin{cases} c_i & \text{i } 1,\ldots,288 \\ \zeta_{i\ 288} & \text{i } 289,\ldots,576 \end{cases}$$

Method IID uses model 4,

$$H_{ji} = \begin{cases} Q_{ij} & \text{i=1,...,288} \\ \chi_{i-288,j} & \text{i=289,...,576} \\ Q^2_{i-576,j} & \text{i=577,...,864} \end{cases}$$

N=864, and the parameters are

$$p_i = \begin{cases} c_i & \text{i=1,...,288} \\ c^0_{i-288} & \text{i=289,...,576} \\ \zeta_{i-576} & \text{i=577,...,864} \end{cases}$$

3 Calibration Performance

All the calibration methods were tested with the same M = 50000 Bhabha events. For methods IA and IB, the minimum total weight required (see sects. 2.1 and 2.2) was W_{min} = 5. Convergence was defined as described in section 2.1, and the maximum number of iterations was set to 80. In the tests reported here, the starting point values of the calibration constants $(c_i)_{i=1}^{288}$ were uniform, random flucuations around the best values as determined by an earlier calibration with method IB with half width 20% of the value. In order to study the convergence properties, the logarithm of $|\Delta S|$ as a function of the iteration number for methods IA and IB for the two calorimeters is plotted in fig. 3. ΔS is defined as the change in $S = \sqrt{\frac{s^2}{M}}$ (see equation 6) from the previous iteration. For both calorimeters method IB shows better convergence. For calorimeter 1 the same conclusion is drawn from fig. 4 which shows the logarithm of the squared step length $step^2 = \sum_i(\Delta c_i)^2$ as a function of the iteration number, where Δc_i denotes the change in the calibration constant of element i from the previous iteration.

The number of elements which did not obtain new calibration constants for method IB, were 20 and 22 for calorimeters 1 and 2, respectively. The corresponding numbers for method IA were 31 and 33. These do not pass the minimum weight criterion. The non-calibrated elements for both calorimeters, method IA and B, are shown in fig. 5. They are all in the shadow of, or bordering, the azimuthal lead mask system. This is true also for the other calorimeter. This problem could be circumvented by changing the criteria of the Bhabha events accepted for use in the calibration algorithm.

Fig. 6 shows the energy (normalized to the beam energy) after the calibration as a function of radius averaged over the two calorimeters. Method IA exhibits a problem in that it tends to overestimate the calibration constant for the elements in the inner ring. In method IB the problem has vanished. The problem with calibration of the inner ring elements is due to the lead mask. The energy deposited in the inner ring of the masked calorimeter for events used by the calibration is the tail of showers of electrons entering the calorimeter outside the

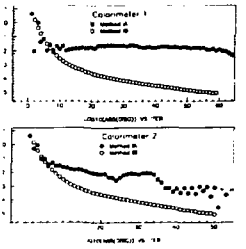

Figure 3: The logarithm of ΔS (see the text) for methods IA and IB in the two calorimeters.

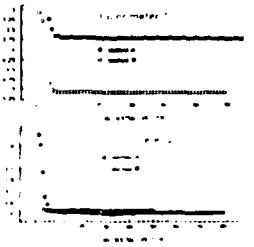

Figure 4: The logarithm of the squared step length (see the text) for methods IA and IB in the two calorimeters.

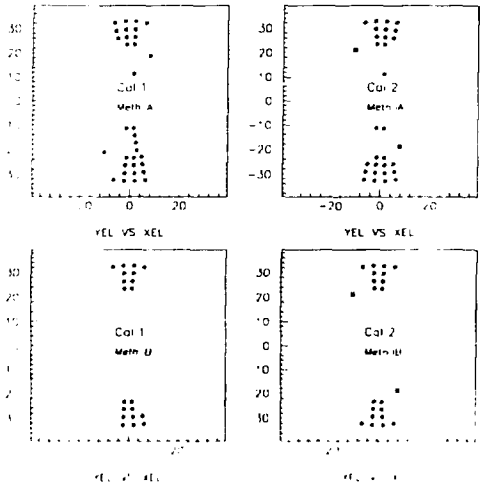

Figure 5: Elements without successfull calibration for the two calorimeters for methods 1A and 1B are marked by a circle. The centre of each readout element is marked by a dot. Dead elements are marked with a star

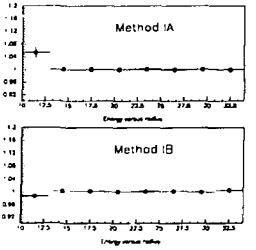

Figure 6: Average reconstructed energy normalized to the expected energy as a function of radius for methods IA and IB. Statistics from both calorimeters.

leadmask. The algorithm of method IB works well in spite of the low energy deposits, whereas method IA overestimates the calibration constants.

The energy distributions obtained in the two calorimeters with calibration methods IA and IB are shown in fig. 7. In the results given below the intrinsic spread in incoming energy has not been corrected for. Gaussians are fitted to the central part of the distributions. The two methods give the same energy resolution, but it should be noted that whereas method IB converged after ~ 60 iterations, method IA did not converge with the strict convergence criterion applied and was stopped after reaching the maximum allowed number of iterations.

The convergence properties of the least squares fit methods are presented in figures 8 and 9. Fig. 8 shows chisquared per degree of freedom, i.e., in the notation of ref. [8] and section 2.3, $F/(M-N)$, as a function of the iteration number.

In fig. 8 only the first 18 iterations, after which method IIA has converged, is shown. Better convergence for method IIA than for the other two is observed. We believe that this is due to the fact that all the parameters of method IIA are of the same type, whereas each of the methods IIB and IIC contains two different classes of parameters. The same conclusion is drawn from fig. 9 where the logarithm of the dimensionless step length $|\Delta e|$ (i.e. the change in the residual e, see ref. [8]) is plotted as a function of the iteration number. It was found essential to use preconditioning (step 4 in section 3 of ref. [8]) to obtain the observed convergence. Method IID has three different classes of parameters and converges even more slowly (not shown in figs. 8 and 9).

As seen from fig. 10 the fit methods do not suffer from anomalies in the radius

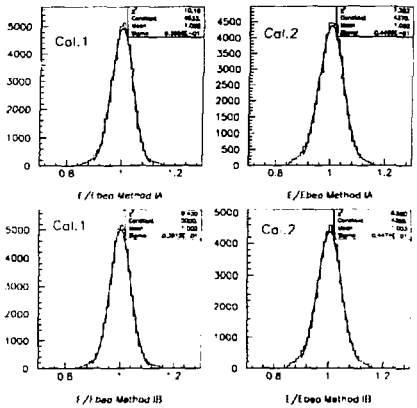

Figure 7: Reconstructed energies after calibration with methods IA and IB for the two calorimeters. Gaussian fits to the central part are performed.

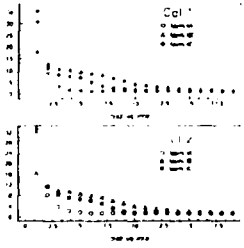

Figure 8: Chisquared per degree of freedom (see the text) plotted as a function of the iteration number for methods IIA, IIB, IIC.

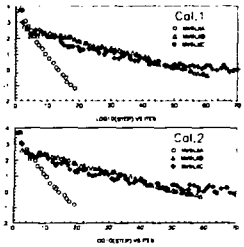

Figure 9: The logarithm of the dimensionless step length (see the text) as a function of the iteration number for the two calorimeters for methods IIA, IIB, IIC.

dependence of the reconstructed energy.

The obtained energy resolutions for the two calorimeters and the six methods are summarized in table 1. The table also contains the number of iterations used. The errors given are the statistical errors from the fit. The cluster energy distributions for method IIA in the two calorimeters are shown in fig. 11.

It is seen from table 1 that while method IIA produces an energy resolution comparable to method IB, methods IIB, IIC, and IID give significantly improved results. Method IID (model 4) is clearly the best one.

The fact that methods IIC and IID give significantly better energy resolution than the other methods is clear evidence of a non-linear energy response. The dimensionless parameter

$$\zeta_i' = \frac{\zeta_i}{c_i^2} < E^{beam} >$$

where $< E^{beam} >$ denotes the average beam energy, is a natural measure of the non-linearity of element i. It is plotted for the elements in calorimeter 1 and 2 after calibration with method IID in fig. 12. Significant negative non-linearities with magnitudes up to 20% are observed. Negative non-linearity parameters mean that the signals increase faster than linearly with energy. The scatter of the parameters is fairly large. It turns out that the non-linearity parameter values are correlated to the detector geometry. No obvious explanation of the sign and size of the observed non-linearity is known to the authors. Also the constant term parameters c_i^2 from a fit with method IID are shown for the two calorimeters in fig. 12. Again significant negative values are observed.

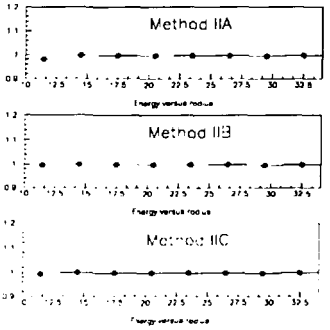

Figure 10: Average reconstructed energy as a function of radius for methods IIA, IIB, and IIC. Statistics from both calorimeters.

Method	Calorimeter	σ_E/E (%)	Number of iterations used
IA	1	3.96±0.02	80 *(max allowed)*
IB	1	3.92±0.02	59
IIA	1	3.88±0.02	18
IIB	1	3.75±0.01	60
IIC	1	3.52±0.01	88
IID	1	3.54±0.01	121
IA	2	4.47±0.02	80 *(max allowed)*
IB	2	4.47±0.02	50
IIA	2	4.43±0.02	18
IIB	2	4.30±0.02	58
IIC	2	4.02±0.02	83
IID	2	3.85±0.02	136

Table 1: Energy resolution and the number of iterations used for the two calorimeters and the six methods.

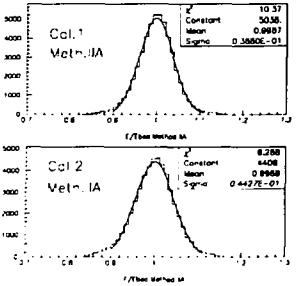

Figure 11: Reconstructed energy after calibration with method IIA in the two calorimeters.

3.1 Stability check.

In order to check the stability of methods IA, IB, and IIA, a new calibration on the same 50000 clusters was run with the output calibration constants from the runs described in the previous section used as input values. The starting values were then perturbed as described in the previous section, but with a new sequence of random numbers. The reconstructed cluster energies obtained with the input and output calibration constants were then compared. Fig. 13 shows the difference (normalized to the beam energy) between the energies in calorimeter 2 (with lead masking) using the input calibration constants and using the constants after the new calibration from perturbed starting values. Note the logarithmic scale.

The clusters in calorimeter 2 with an energy difference greater than 2% of the beam energy (45, 50, and 33 for methods IA, IB, and IIA, respectively) are situated behind or neighbouring the lead mask or close to the outer acceptance border. This is shown for method IIA in fig. 14

Furthermore, the stability of the number of Bhabha events accepted by the Bhabha analysis was checked using the different sets of calibration constants. The results are summarized in table 2. It is seen that for all three methods the stability is better than 0.05%, and that the difference between the two well converging methods IB and IIA also is of the order 0.05%.

An independent check of the absolute stability of Method IB was performed on a set of simulated Bhabha events. During the simulation the energy deposited into each readout element was converted to ADC counts using the nominal cal-

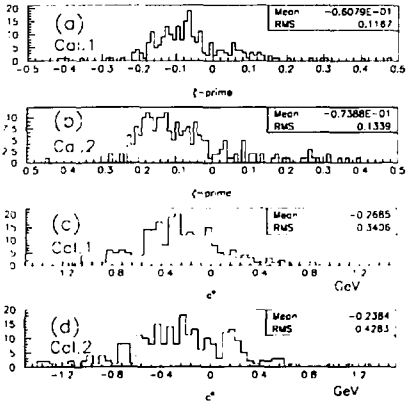

Figure 12: The non-linearity parameters ζ' (see the text) from a fit with method IID are shown for calorimeter 1 and 2 in (a) and (b), respectively. The constant term parameters from the same fit are shown in (c) and (d).

Method	Nb of Bhabhas	
	1st calibration	2nd calibration
IA	103230	103193
IB	103296	103304
IIA	103240	103238

Table 2: The number of accepted Bhabha events after 1st and 2nd calibration (with perturbed start values, see the text) with methods IA, IB, IIA.

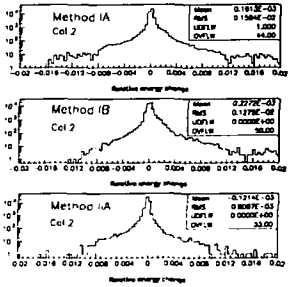

Figure 13: The difference of reconstructed cluster energies between two successive calibrations (see the text) for methods IA, IB, and IIA. The differences are normalized to the beam energy.

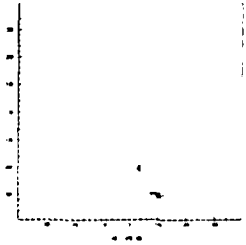

Figure 14: The position of energy clusters in calorimeter 2 (with lead masking) with more than 2% change in the reconstructed energy between two successive calibrations with method IIA. The centre of readout elements are marked with dots.

ibration constants found with the real data. These simulated "raw" data were then passed through the event reconstruction and Bhabha event selection with the same calibration constants in order to determine the nominal number of accepted simulated events. A re-calibration of the simulated detector with method IB resulted in a decrease in the number of accepted events of $(0.07 \pm 0.02)\%$. An additional re-calibration was performed on a sample of simulated events in which 90% of the collinear events (no radiative photon, i.e. both e^+ and e^- have exactly the beam energy) away from the detector edges were excluded. Despite the poor quality of the remaining events for calibration purposes, this resulted in only an additional 0.03% reduction in the number of accepted simulated events.

4 Summary and conclusions

Six algorithms for *in situ* absolute energy calibration of the readout elements of two electromagnetic calorimeters used for luminosity measurement by Bhabha event counting at LEP have been presented. Two of them, methods IA and IB, are simple *ad hoc* iterative methods, based on the model of eq. 1. The four other methods, IIA, IIB, IIC, and IID, are based on linear least squares fits using the four models of eqs. 1, 2, 3, and 4, respectively.

The pre-conditioned conjugate gradient method was used for solving the least squares problem numerically, see ref. [8] for details. This is a simple, robust and efficient method for problems like the present one which are large, with a sparse coefficient matrix, and likely to be ill-conditioned.

The six methods have been tested for convergence properties and resulting energy resolution. Furthermore, the stability properties of methods IA, IB, and IIA have been studied in detail.

Methods IB and IIA give comparable energy resolution. For equivalent convergence criteria method IIA converges faster than method IB. Method IA fails to converge and produces anomalous reconstructed energy in the readout elements behind the lead mask. Methods IIB and IIC show similar convergence properties to method IB, but significantly better energy resolution, in particular this is true for method IIC which uses a model quadratic in the ADC signals. This is clear evidence of a non linear energy response. Method IID converges more slowly than methods IIB and IIC, but gives an improved energy resolution.

References

[1] P.Abreu et al.(The DELPHI coll.), **Nucl.Phys.B367(1991)511**.

[2] L.Bugge et al.,*DELPHI SAT Luminosity Analysis: 1990*, DELPHI 91-104 PHYS 147, 1 November 1991 (unpublished).

L.Bugge et al.,*Preliminary SAT Luminosity Analysis: 1991*, DELPHI 91-81 CAL 81 PHYS 133, 21 August 1991 (unpublished).

[3] P.Aarnio et al.(The DELPHI coll.), **Nucl.Instr.Meth.A303**(1991)233.

[4] S.J.Alvsvåg et al., **Nucl.Instr.Meth.A290**(1990)320.

[5] M.Böhm, R.Kleiss and W.Hollik, **Nucl.Phys.B304**(1988)687.
F.A.Berends, W.Hollik and R.Kleiss, **Nucl.Phys.B304**(1988)712.

[6] G.H. Golub and C.F. van Loan, *Matrix Computations*,
North Oxford Academic, London (1986).

[7] W.H. Press, B.P. Flannery, S.A. Teukolsky and W.T. Vetterling,
Numerical Recipes, The Art of Scientific Computing,
Cambridge University Press, Cambridge (1989).

[8] J.Myrheim, H.Rue and L.Bugge, *A Simple Algorithm for Large, Non-Linear or Singular Least Squares Problems*, University of Oslo preprint, Dept.of physics, Report 92-19, 1992, to be submitted to Nucl.Instr.Meth.A.

FYSISK INSTITUTT FORSKNINGS-GRUPPER	DEPARTMENT OF PHYSICS RESEARCH SECTIONS
Biofysikk	Biophysics
Elektronikk	Electronics
Elementærpartikkel-fysikk	Experimental Elementary Particle physics
Faste stoffers fysikk	Condensed Matter physics
Kjernefysikk	Nuclear physics
Plasma-, molekylar- og kosmisk fysikk	Plasma-, Molecular and Cosmic physics
Strukturfysikk	Structural physics
Teoretisk fysikk	Theoretical physics

ISBN